INSTITUTE OF PHYSICS PUBLISHING PLASMA PHYSICS AND CONTROLLED FUSION

Plasma Phys. Control. Fusion **46** (2004) 1271–1282 PII: S0741-3335(04)75437-8

Microwave imaging reflectometry for the measurement of turbulent fluctuations in tokamaks

E Mazzucato

Princeton Plasma Physics Laboratory, Princeton, NJ 08543, USA

E-mail: mazzucato@pppl.gov

Received 29 January 2004
Published 24 June 2004
Online at stacks.iop.org/PPCF/46/1271
doi:10.1088/0741-3335/46/8/008

Abstract

This paper describes a numerical study of microwave reflectometry for the measurement of turbulent fluctuations in tokamak-like plasmas with a cylindrical geometry. Similarly to what was found previously in plane-stratified plasmas, the results indicate that the characteristics of density fluctuations cannot be uniquely determined from the reflected waves if the latter are allowed to propagate freely to the point of detection, as in standard reflectometry. Again, we find that if the amplitude of fluctuations is below a threshold that is set by the spectrum of poloidal wave numbers, the local characteristics of density fluctuations can be obtained from the phase of the reflected waves when these are collected with a wide aperture antenna, and an image of the cut-off is formed onto an array of phase-sensitive detectors.

1. Introduction

Microwave reflectometry [1], a radar technique for the detection of fluctuations using the reflection of electromagnetic waves from a plasma cut-off, has found extensive use for the detection of short-scale turbulent fluctuations in tokamaks—the probable cause of anomalous transport in this type of magnetic configurations [2, 3]. However, the extraction of any quantitative information from the measured signals is always very difficult and often impossible. This is caused by two phenomena. First, the high sensitivity of reflectometry to plasma fluctuations makes its response non-linear, as demonstrated by the very first application of this technique to tokamaks [4]. The second reason, which is more subtle and was not promptly understood [5], is due to the fact that when the plasma permittivity fluctuates perpendicularly to the direction of propagation of the probing beam, as in the case of tokamak plasmas, where turbulent fluctuations vary in both radial and poloidal directions, the spectral components of the backward wave propagate in different directions. This may result in a complicated interference pattern on the detection plane, from which it is very difficult to extract any quantitative information about the fluctuations under investigation.

This can be understood by considering a simple case where the wave permittivity has the form $\varepsilon = \varepsilon_0(r) + \tilde{\varepsilon}(r,\theta)$ (where $\tilde{\varepsilon} \ll 1$ is the fluctuating component and (r,θ) is a system of coordinates representing the radial and poloidal directions of a tokamak plasma), and by assuming that the reflected wave near the cut-off can be cast in the form $E = \exp(\mathrm{i}\tilde{\phi})$, with $\tilde{\phi}(\theta)$ given by the geometric optics approximation (*phase screen model*) [5, 6]. Since the phase of the probing wave is the cumulative result of many random contributions, we may assume that $\tilde{\phi}(\theta)$ is a normal random variable with mean $\langle\tilde{\phi}\rangle = 0$, variance $\sigma_\phi^2 \equiv \langle\tilde{\phi}^2\rangle$ and autocorrelation $\gamma_\phi(\delta) \equiv \langle\tilde{\phi}(\theta)\tilde{\phi}(\theta+\delta)\rangle/\sigma_\phi^2$. From this, we find that the first moment of the wave amplitude (i.e. the amplitude of the coherent specular reflection) is $\langle E\rangle = \exp(-\sigma_\phi^2/2)$, and thus it is a decreasing function of σ_ϕ. From the joint probability density [7]

$$P(\tilde{\phi}_1,\tilde{\phi}_2) = \frac{1}{2\pi\sigma_\phi^2(1-\gamma_\phi^2)^{1/2}}\exp\left[-\frac{\phi_1^2 - 2\gamma_\phi\phi_1\phi_2 + \phi_2^2}{2\sigma_\phi^2(1-\gamma_\phi^2)}\right], \tag{1}$$

where $\tilde{\phi}_1 \equiv \tilde{\phi}(\theta)$ and $\tilde{\phi}_2 \equiv \tilde{\phi}(\theta+\delta)$, we get the second moment of the wave amplitude $\langle E_1 E_2^*\rangle = \exp[-\sigma_\phi^2(1-\gamma_\phi)]$, which shows that the signal correlation length is also a decreasing function of σ_ϕ. The normalized autocorrelation of E is then given by

$$\gamma_E \equiv \frac{\langle\tilde{E}_1\tilde{E}_2^*\rangle}{\langle|\tilde{E}|^2\rangle} = \frac{\mathrm{e}^{\sigma_\phi^2\gamma_\phi} - 1}{\mathrm{e}^{\sigma_\phi^2} - 1}. \tag{2}$$

From this, we get $\gamma_E \approx \gamma_\phi$ for $\sigma_\phi^2 \ll 1$. On the other hand, for $\sigma_\phi^2 \gg 1$, by taking $\gamma_\phi \approx \exp(-\delta^2/2\Delta_\phi^2)$ and making the approximation $\gamma_\phi \approx 1 - \delta^2/2\Delta_\phi^2$ for $\delta^2 \ll \Delta_\phi^2$, we obtain $\gamma_E \approx \exp(-\delta^2\sigma_\phi^2/2\Delta_\phi^2)$. To summarize, when $\sigma_\phi^2 \gg 1$, the correlation length of the wave amplitude is a factor of σ_ϕ smaller than the correlation length of $\tilde{\phi}$.

In conclusion, γ_ϕ cannot be derived from the measured value of γ_E without a knowledge of σ_ϕ. On the other hand, the latter cannot be measured when the reflected waves are allowed to propagate freely to the detection plane, where they may form a chaotic interference pattern. In a series of papers [8–10], the author has discussed the possibility of overcoming this difficulty by collecting the reflected waves with a wide aperture optical system forming an image of the cut-off onto an array of phase sensitive detectors. This should allow a measurement of the autocorrelation function γ_ϕ, and hence information on the structure of plasma density fluctuations near the cut-off. Such a reflectometry scheme—named microwave imaging reflectometry—was the result of an extensive series of numerical simulations where, as in the previous paragraph, a plane-stratified plasma equilibrium was used in conjunction with a field of two-dimensional fluctuations. In this paper, we re-analyse the same problem using a plasma equilibrium configuration with a more realistic cylindrical geometry.

2. Physical model

We assume that the density (n) of a cylindrically symmetric plasma is perturbed by a field of two-dimensional density fluctuations ($\tilde{n}$) with the spatial distribution

$$\frac{\tilde{n}(r,\theta)}{n(r)} = \sum_{p=1}^{P}\sum_{q=1}^{Q}\delta_{pq}\cos(p\kappa r + \varphi_{pq})\cos(q\theta) \tag{3}$$

in the system of cylindrical coordinates (r, θ). This spectrum consists of $P \times Q$ discrete components with radial wave number $k_r = p\kappa$ ($\kappa \equiv$ constant), poloidal number q, random phase φ_{pq} and amplitudes δ_{pq}. As in previous simulations [8, 9], the rationale for choosing

a poloidally symmetric spectrum of fluctuations is that it provides an extra check for the calculated reflected wave, which obviously must display the same degree of symmetry. However, the numerical code used in this paper could deal with odd symmetric fluctuations as well, with results that are substantially similar to those described in this paper.

Similarly to [8], we take the amplitude distribution

$$\delta_{pq}^2 \propto p \exp\left[-\left(\frac{p\kappa}{\kappa_r}\right)^2 - \left(\frac{q}{q_0}\right)^2\right], \tag{4}$$

where the constants $\kappa_r = \kappa P/2$ and q_0 represent the spectral width of fluctuations in the radial and poloidal directions, respectively. At the cut-off, the poloidal spectral width can also be expressed in terms of the wave number $\kappa_p = q_0/r_c$. Throughout this paper we will use $P = 21$ and $Q = 101$.

The probing wave is launched from $r = r_0$ with the Gaussian amplitude profile

$$E_0(\theta) = \mathrm{e}^{-(\theta/\theta_0)^2}, \tag{5}$$

where θ_0 is a constant. Since we assume $\theta_0 \ll \pi$, equation (5) can also be cast in the form

$$E_0(\theta) \approx \frac{\theta_0}{2\sqrt{\pi}} \sum_{m=-\infty}^{m=+\infty} \mathrm{e}^{-(m\theta_0/2)^2}\mathrm{e}^{\mathrm{i}m\theta} \equiv \sum_{m=-\infty}^{m=+\infty} g_m \mathrm{e}^{\mathrm{i}m\theta}. \tag{6}$$

The total amplitude (E) of the wave, which we will assume propagating in the ordinary mode, is expressed as the sum of $2N + 1$ independent solutions of the wave equation

$$E(r,\theta) = \sum_{n=-N}^{N} c_n E_n(r,\theta), \tag{7}$$

where $N \gg Q$ (to be determined). The functions E_n are cast in the form

$$E_n(r,\theta) = \sum_{m=-N}^{N} f_{mn}(r)\mathrm{e}^{\mathrm{i}m\theta}, \tag{8}$$

where $f_{mn}(r)$ are solutions of the system of $2N + 1$ ordinary differential equations

$$\frac{\mathrm{d}^2 f_{mn}}{\mathrm{d}r^2} + \frac{1}{r}\frac{\mathrm{d}f_{mn}}{\mathrm{d}r} + k_0^2(\varepsilon_0 - \alpha_m^2) f_{mn} + k_0^2(\varepsilon_0 - 1) \times \sum_{p=1}^{P}\sum_{q=1}^{Q}\left[\frac{\delta_{pq}}{2}\cos(p\kappa r + \varphi_{pq})(f_{(m-q)n} + f_{(m+q)n})\right] = 0 \quad (m = -N, -N+1, \ldots, N) \tag{9}$$

with $\varepsilon_0 = 1 - (\omega_p/\omega)^2$ (the unperturbed permittivity), $\omega_p = (4\pi n e^2/m_e)^{1/2}$ (the plasma frequency), $\alpha_m = m/k_0 r$ and $k_0 = \omega/c$ (the probing wave number). These equations, which are derived by inserting equations (3) and (8) into the wave equation and by performing a Fourier expansion in θ, can be solved using the Runge–Kutta method.

The coefficients c_n in equation (7) are obtained by imposing the condition that the wave field at $r = r_0$ is the sum of the incoming probing wave (equation (6)) and an outgoing reflected wave

$$E_r(\theta) = \sum_{m=-N}^{N} a_m \mathrm{e}^{\mathrm{i}m\theta}. \tag{10}$$

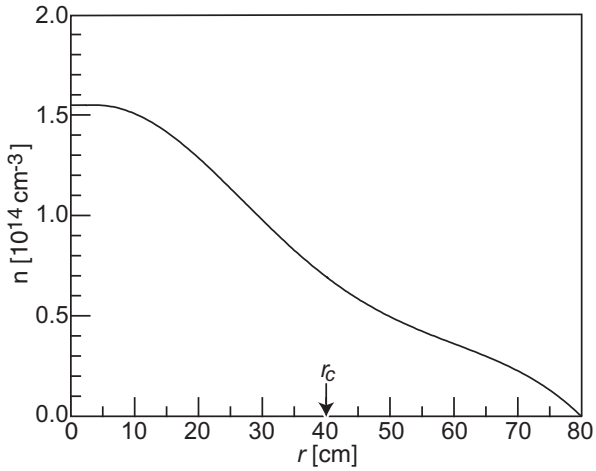

Figure 1. Plasma density profile; the cut-off is at $r = r_c$ for a probing wave with a frequency of 75 GHz and the ordinary mode of propagation.

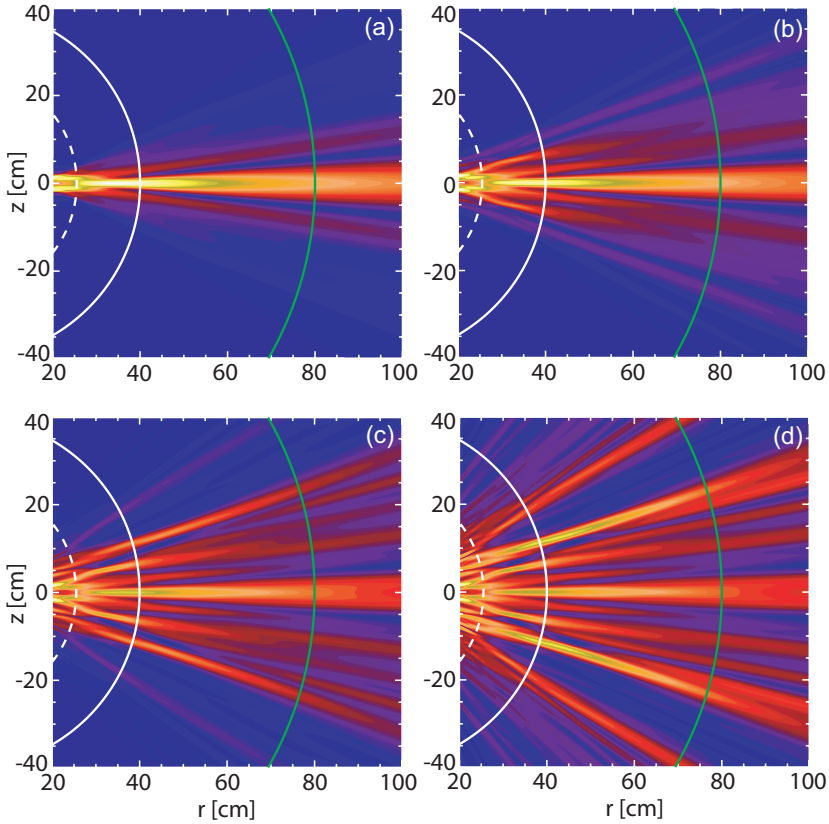

Figure 2. Contour plots of $|E_b|$ for different values of the angular width θ_0: 5° (*a*), 10° (*b*), 20° (*c*), 40° (*d*). Green line is the plasma boundary ($r_b = 80$ cm), solid white line is the cut-off ($r_c = 40$ cm), dashed line is the virtual cut-off ($r_G = 26$ cm). Fluctuations parameters: $q_0 = 40$, $\kappa_r = 1.0\,\mathrm{cm}^{-1}$ and $\sigma_n = 1.0 \times 10^{-2}$.

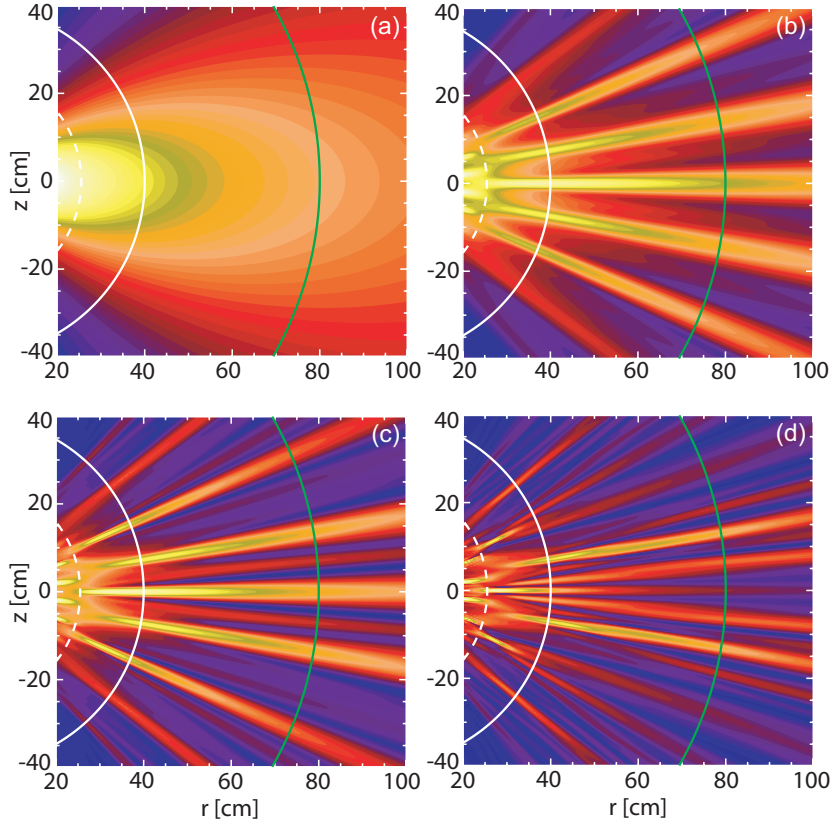

Figure 3. Contour plots of $|E_b|$ for different values of σ_n: 0.0 (*a*), 0.5×10^{-2} (*b*), 1.0×10^{-2} (*c*), 2.0×10^{-2} (*d*). Other parameters: $q_0 = 20$, $\kappa_r = 1.0\,\mathrm{cm}^{-1}$, $\theta_0 = 40^\circ$.

From this we get a first set of $2N + 1$ equations

$$\sum_{n=-N}^{N} f_{mn}(r_0)c_n - a_m = g_m \qquad (m = -N, -N+1, \ldots, N). \tag{11}$$

Another set of equations can be derived from the expressions

$$E_f(r,\theta) = \sum_{m=-\infty}^{m=\infty} g_m \frac{H_m^{(2)}(k_0 r)}{H_m^{(2)}(k_0 r_0)} \mathrm{e}^{\mathrm{i}m\theta} \tag{12}$$

and

$$E_b(r,\theta) = \sum_{m=-N}^{N} a_m \frac{H_m^{(1)}(k_0 r)}{H_m^{(1)}(k_0 r_0)} \mathrm{e}^{\mathrm{i}m\theta}, \tag{13}$$

representing the solutions of the wave equation, which, at $r = r_0$, coincide with equations (6) and (10), respectively. In these expressions, $H_m^{(1)} \equiv J_m + \mathrm{i}Y_m$ and $H_m^{(2)} \equiv J_m - \mathrm{i}Y_m$ are the *Hankel* functions [11] which satisfy the recurrence relation

$$2F_m'(z) = F_{m-1}(z) - F_{m+1}(z).$$

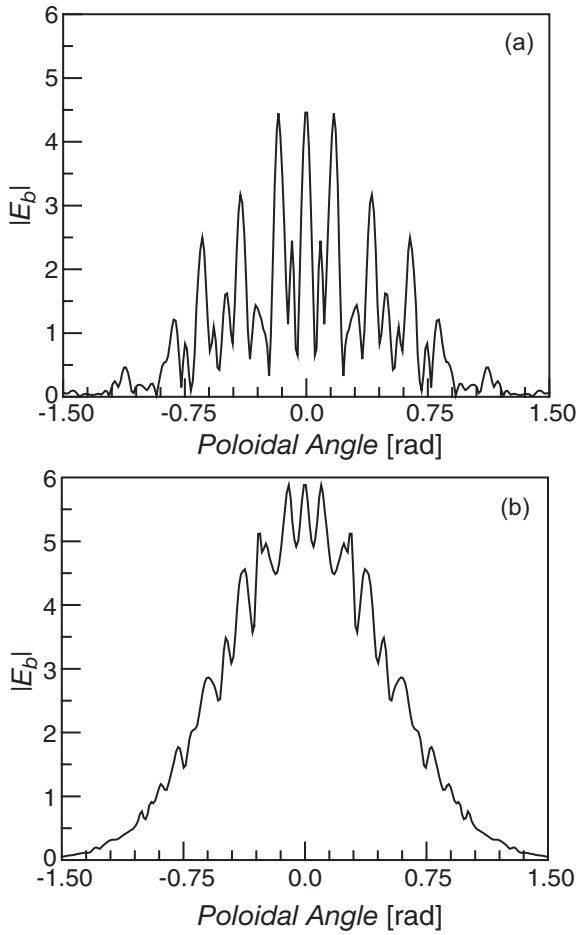

Figure 4. Profile of $|E_b|$ at $r = r_0$ (a) and $r = r_G$ (b) for the case of figure 3(c).

From the r-derivatives, then, we obtain a second set of equations

$$\sum_{n=-N}^{N} f'_{mn}(r_0)c_n - \frac{a_m k_0 H_m^{(1)'}(k_0 r_0)}{H_m^{(1)}(k_0 r_0)} = \frac{g(m)k_0 H_m^{(2)'}(k_0 r_0)}{H_m^{(2)}(k_0 r_0)} \qquad (m = -N, -N+1, \ldots, N), \tag{14}$$

which together with equation (11) determine the values of a_n and c_n.

In the following, equation (13) will be referred to as the backward field. Outside of the plasma region, E_b coincides with the reflected wave, while inside the plasma region, it represents a virtual field that an observer in free space could measure by using an optical system to map the plasma region onto an array of detectors located at the image plane.

Finally, the integer N must be chosen large enough to make the results significantly unchanged by any increase in its value. This condition, verified *a posteriori*, allows the closure of the system of equations by setting to zero all terms $f_{(m\pm q)n}$ with $|m \pm q| > N$. The numerical simulations of this paper have been performed using values of N in the range $200 \leqslant N \leqslant 250$.

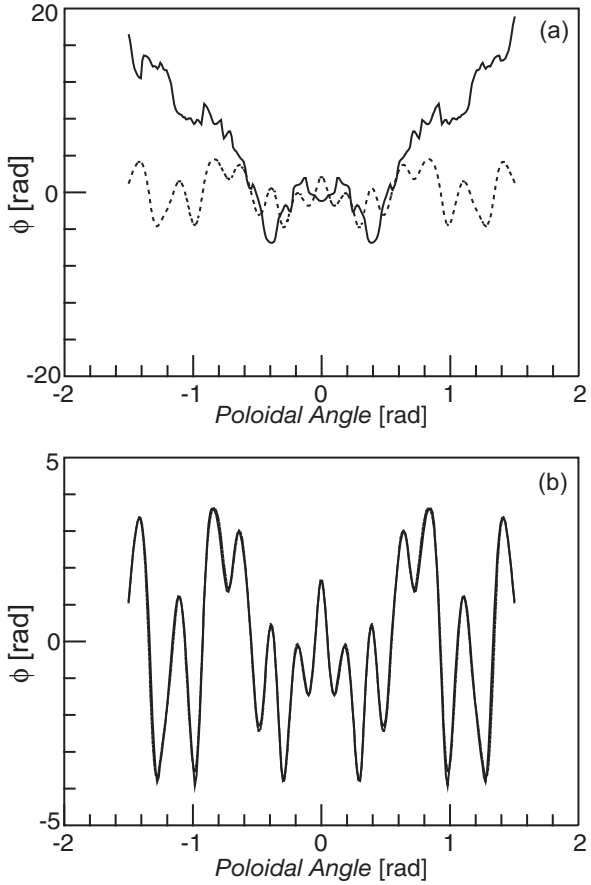

Figure 5. Comparison of $\tilde{\phi}$ (——) and $\tilde{\phi}_{GO}$ (- - - -) at $r = r_0$ (*a*) and $r = r_G$ (*b*) for the case of figure 3(*c*). Note that the two curves in the bottom figure are almost identical.

3. Numerical results

The numerical results described in this section refer to the case of a cylindrical plasma with a radius of $r_b = 80\,\mathrm{cm}$ and the density profile of figure 1 (derived from a typical plasma equilibrium of the tokamak fusion test reactor [5]). The probing wave has a frequency of 75 GHz and is launched from $r_0 = 100\,\mathrm{cm}$. The cut-off has a radius of $r_c = 40\,\mathrm{cm}$ where the density scale length is $L_n \equiv n/(\mathrm{d}n/\mathrm{d}r) = 25\,\mathrm{cm}$.

Figure 2 displays the contour plot of the backward field amplitude $|E_b|$ for different values of the angular aperture of the probing beam (θ_0). The field of turbulent fluctuations is the same in all four cases, with $\sigma_n \equiv \langle \tilde{n}^2/n^2 \rangle^{1/2} = 1.0 \times 10^{-2}$, $\kappa_r = 1.0\,\mathrm{cm}^{-1}$ and $q_0 = 40$ ($\kappa_p = 1.0\,\mathrm{cm}^{-1}$). Figure 3 displays similar plots for a constant beam aperture ($\theta_0 = 40^\circ$) but different values of σ_n. In all four cases, the fluctuations have the same value of $q_0 = 20$ ($\kappa_p = 0.5\,\mathrm{cm}^{-1}$) and $\kappa_r = 1.0\,\mathrm{cm}^{-1}$, and identical sets of random phases (φ_{pq}).

The plots of figures 2 and 3 illustrate how the radiation pattern of the backward field splits into several striations that seem to originate from a location behind the cut-off—a *virtual cut-off*—where the fluctuations in the backward field amplitude are at their minimum. As noted in the previous section, the backward field does not coincide with the reflected wave in the

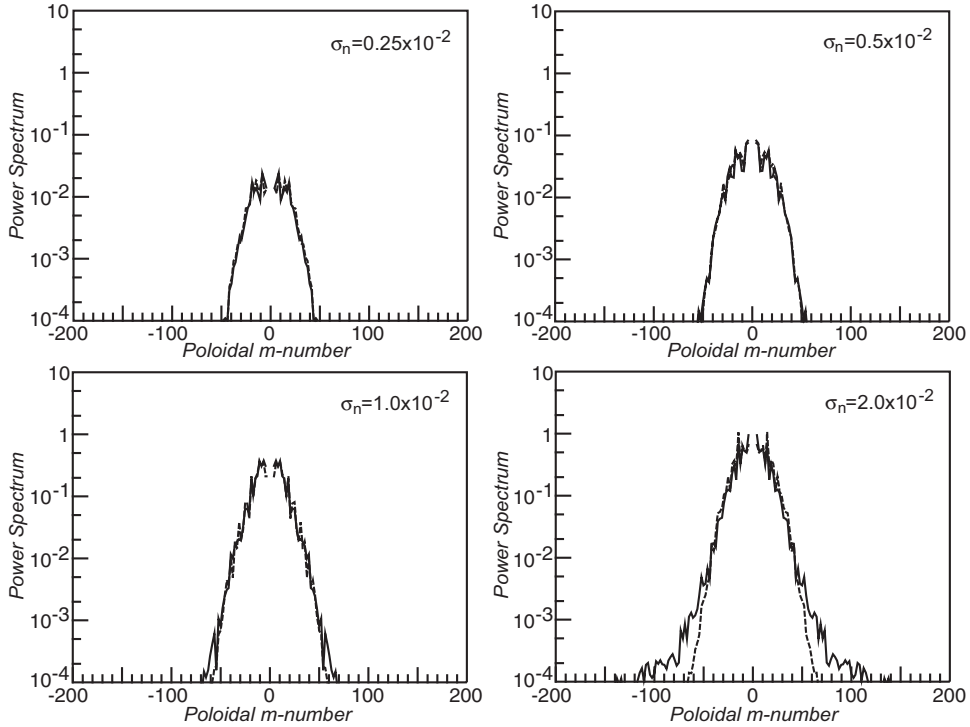

Figure 6. Power spectra of $\tilde{\phi}$ at $r = r_G$ (——) and of $\tilde{n}/n$ at $r \approx r_c$ (- - - -) for different values of σ_n. Other parameters are those of figure 3. Spectra are averaged over twenty realizations of the turbulence field.

plasma region. It is simply how the reflected wave, after crossing the region between the cut-off and the plasma edge, would appear to an observer in free space. Since the refractive index of this region is lower than one, the striations seem to start from a radial location (r_G) behind the cut-off, at a distance from the latter of the order of the density scale length (L_n), i.e. where the rays of waves originating near the real cut-off seem to intersect when observed in free space. This phenomenon is similar to what makes the bottom of a swimming pool to appear artificially close to the surface, the only difference in this case being a refractive index larger than one. In figures 2 and 3, the distance between the real and the virtual cut-off is approximately half ($\sim L_n/2$) of what was found ($\sim L_n$) previously in plane geometry [8, 9]. This is explained by the fact that in a cylindrical plasma the conservation of the poloidal m-number causes a strong bending in the rays of reflected waves, which therefore appear to originate closer to the cut-off than in a plane plasma configuration with similar density gradients.

As described in the introduction, interference of the spectral components of the reflected wave may result in a chaotic wave pattern in free space—the only place where we can perform reflectometry measurements. This is demonstrated in figure 4(a), which shows that the amplitude of the backward field at $r = r_0$ is strongly modulated by the fluctuations of figure 3(c). Furthermore, the fluctuating component ($\tilde{\phi}$) of the phase of E_b (i.e. the change in the phase of the backward field due to the presence of fluctuations) is completely different from the phase of geometric optics $\tilde{\phi}_{GO}(\theta) = k_0 \int_{r_c}^{r_b} \tilde{\varepsilon}/\sqrt{\varepsilon_0}\, \mathrm{d}r$ (figure 5(a)). In contrast, plasma fluctuations have a small effect on the value of $|E_b|$ near the virtual cut-off (figure 4(b)), where $\tilde{\phi}$ coincides with $\tilde{\phi}_{GO}$ (figure 5(b)). Consequently, since most of the contribution to $\tilde{\phi}_{GO}$ comes from a narrow region in front of the cut-off, the poloidal power spectrum of $\tilde{\phi}$ at $r = r_G$ must

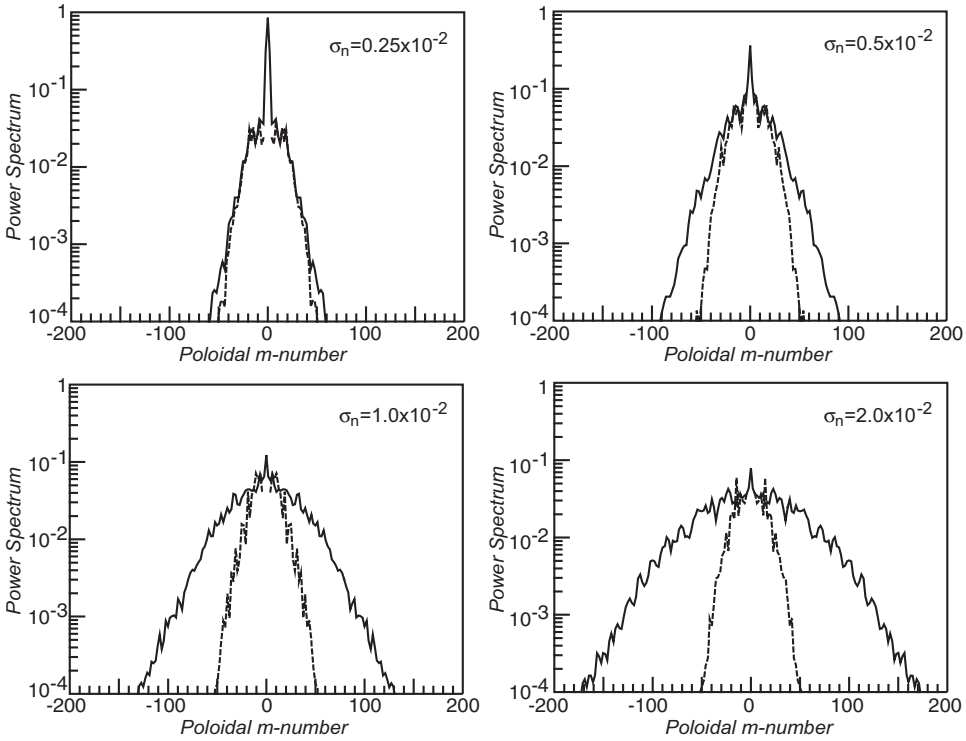

Figure 7. Power spectra of E_b at $r = r_0$ (——) and of $\tilde{n}/n$ at $r \approx r_c$ (- - - -) for the fluctuations of figure 6. Spectra are averaged over twenty realizations of the turbulence field (density spectra are renormalized).

be similar to that of $\tilde{n}/n$ at $r = r_c$. This is indeed the case, as demonstrated in figure 6 where the spectrum of $\tilde{n}/n$ is normalized by the factor $\kappa_r/\pi k_0^2 L_n$ (derived from the approximation of geometric optics [5, 6]). Similarly to the results of previous simulations [9], we find that the best agreement is obtained using the value of $\tilde{n}/n$ at a small distance from the cut-off (∼0.5 cm in figure 6).

Apart from a few rare cases, such as that of [5], a normal procedure of standard reflectometry is to identify the spectrum of plasma turbulence with the spectrum of measured signals. This leads to erroneous results, as demonstrated by figure 7 showing the power spectra of E_b at $r = r_0$ and of $\tilde{n}/n$ at $r = r_c$ (the latter being renormalized for facilitating the comparison with the backward field spectra). These results show very clearly that, as plasma fluctuations rise to the level found in tokamaks, the spectrum of reflected waves in free space—the main product of standard reflectometry—becomes considerably broader than the spectrum of fluctuations.

As in previous simulations [8, 9], we find that the possibility of inferring the spectrum of plasma turbulence from the phase of the backward field breaks down at large levels of plasma fluctuations. This is explained by the fact that, since each spectral component of the backward wave originates near the corresponding reflecting point, the breakdown occurs when the set of these points is distributed over a distance δr that is comparable to the radial scale of plasma fluctuations (κ_r^{-1}). This occurs when [8, 9]

$$\sigma_n < \frac{1}{\pi^{3/4} L_n \kappa_p}. \tag{15}$$

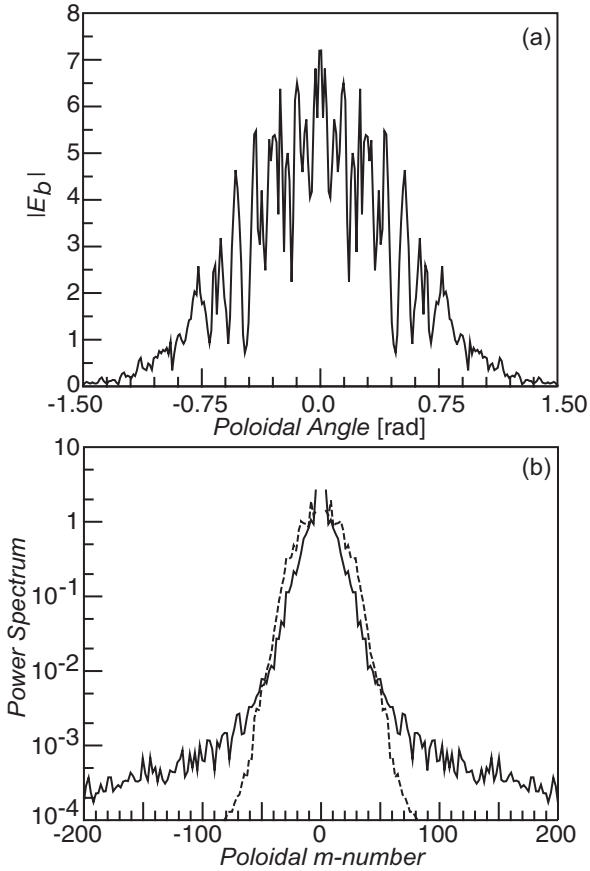

Figure 8. (*a*) Profile of $|E_b|$ at $r = r_G$. (*b*) Poloidal power spectrum of $\tilde{\phi}$ at $r = r_G$ (——) and of $\tilde{n}/n$ at $r \approx r_c$ (- - - -). Parameters are those of figure 3 with $\sigma_n = 3.0 \times 10^{-2}$. Spectra are averaged over twenty realizations of the turbulence field.

When this condition is not satisfied, we expect large fluctuations in the value of $|E_b|$ at the virtual cut-off and a departure of the spectrum of $\tilde{\phi}$ (at $r = r_G$) from that of $\tilde{n}/n$ (at $r = r_c$). This is indeed what figure 8 shows when the value of σ_n is raised to 3.0×10^{-2} for fluctuations similar to those of figure 6 ($\kappa_p = 0.5\,\mathrm{cm}^{-1}$ and $L_n = 25\,\mathrm{cm}$), in agreement with equation (15) that gives $\sigma_n < 3.4 \times 10^{-2}$. Another demonstration of the validity of this criterion is provided by figure 9, where the breakdown occurs for a value of σ_n smaller than 2×10^{-2} when $\kappa_p = 1.0\,\mathrm{cm}^{-1}$, again in agreement with equation (15), which for this case gives $\sigma_n < 1.7 \times 10^{-2}$. The contour plot of $|E_b|$ in figure 10 shows that this is accompanied by the destruction of the virtual cut-off.

Finally, it is worth noting that when equation (15) is not satisfied, such as in figures 8(*b*) and 9(*b*), the power spectrum of $\tilde{\phi}$ acquires a $1/m^2$ dependence, which is reminiscent of the $1/f^2$ frequency dependence of the spectra of standard reflectometry [1, 6].

4. Conclusion

In conclusion, we have presented a numerical study of microwave reflectometry for the measurement of turbulent fluctuations in a tokamak-like plasma with a cylindrical equilibrium

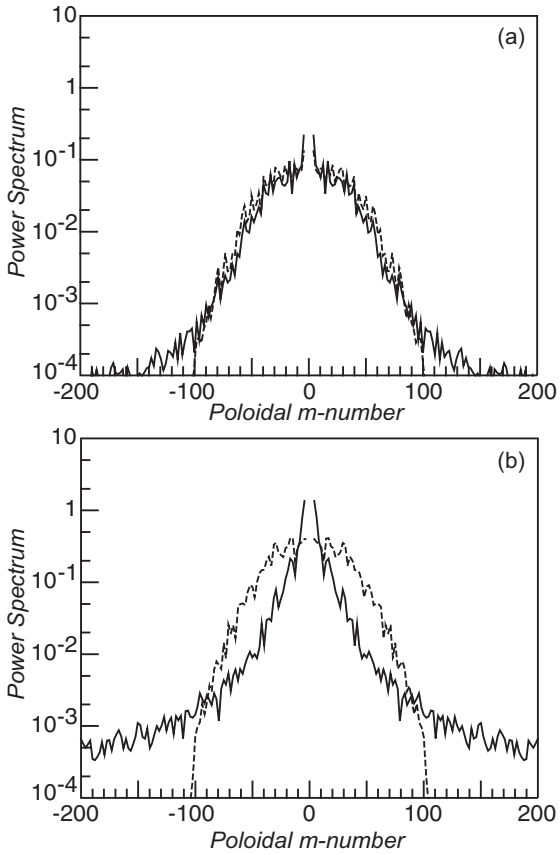

Figure 9. Same as in figure 8(*b*) for $q_0 = 40$, $\kappa_r = 1.0\,\mathrm{cm}^{-1}$, $\sigma_n = 1.0 \times 10^{-2}$ (*a*) and $\sigma_n = 2.0 \times 10^{-2}$ (*b*). Spectra are averaged over twenty realizations of the turbulence field.

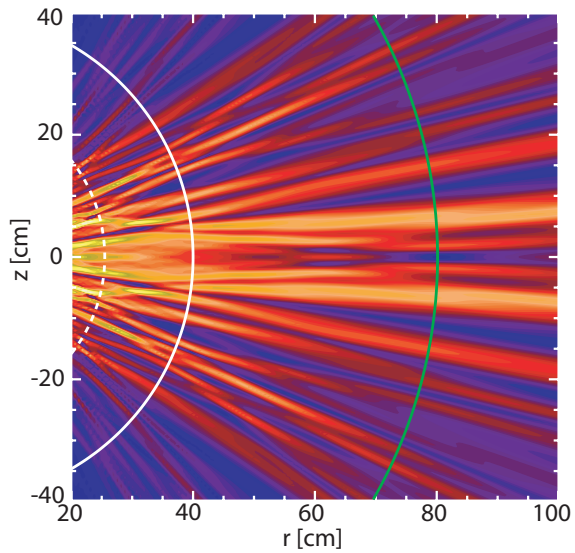

Figure 10. Contour plots of $|E_b|$ for the case of figure 9(*b*).

configuration. Similarly to what was found previously in plane-stratified configurations, our results indicate that the characteristics of plasma fluctuations cannot be uniquely determined from the reflected waves if these are allowed to propagate freely to the point of detection, as in standard reflectometry. Again, we find that if the amplitude of fluctuations is below a threshold that is set by the spectrum of poloidal wave numbers (equation (15)), the local characteristics of density fluctuations can be obtained from the phase of reflected waves when these are collected with a wide aperture antenna and an image of the cut-off is formed (taking into account plasma refraction) onto an array of phase sensitive detectors. A reflectometer apparatus for testing this conjecture has been constructed and is currently being commissioned on the TEXTOR tokamak [12, 13].

Acknowledgments

The author wishes to thank T Munsat for useful discussions and for help in the visualization of numerical results. This work was supported by US DOE Contract No DE-AC02-76-CHO-3073.

References

[1] Mazzucato E 1998 *Rev. Sci. Instrum.* **69** 2201
[2] Horton W 1999 *Rev. Mod. Phys.* **71** 735
[3] Connor J W and Wilson H R 1994 *Plasma Phys. Control. Fusion* **36** 719
[4] Mazzucato E 1975 *Bull. Am. Phys. Soc.* **20** 1241
Mazzucato E 1975 *PPPL* MATT-1151
[5] Mazzucato E and Nazikian R 1993 *Phys. Rev. Lett.* **71** 1840
[6] Nazikian R and Mazzucato E 1995 *Rev. Sci. Instrum.* **66** 392
[7] Davenport W B and Root W L 1958 *Random Signals and Noise* (New York: McGraw-Hill)
[8] Mazzucato E 1998 *Rev. Sci. Instrum.* **69** 1691
[9] Mazzucato E 2001 *Nucl. Fusion* **41** 203
[10] Mazzucato E, Munsat T, Park H, Deng B H, Domier C W, Luhmann N C Jr, Donné A J H and van de Pol M J 2002 *Phys. Plasmas* **9** 1955
[11] Abramowitz M and Stegun I A 1965 *Handbook of Mathematical Functions* (New York: Dover)
[12] Munsat T, Mazzucato E, Park H, Deng B H, Domier C W, Luhmann N C Jr, Wang J, Xia Z G, Donné A J H and van de Pol M J 2003 *Rev. Sci. Instrum.* **74** 1426
[13] Munsat T, Mazzucato E, Park H, Domier C W, Luhmann N C, Donné A J H and van de Pol M J 2003 *Plasma Phys. Control. Fusion* **45** 469